

## RESEARCH ARTICLE

10.1002/2013JF002900

## Key Points:

- Plant, flow and sediment interaction in response to various initial bathymetry
- Plant-flow interactions drive landscape development at initial flat bathymetry
- Initial bathymetry is able to influence the magnitude of plant-flow interactions

## Correspondence to:

C. Schwarz,  
christian.schwarz@nioz.nl

## Citation:

Schwarz, C., Q. H. Ye, D. van der Wal, L. Q. Zhang, T. Bouma, T. Ysebaert, and P. M. J. Herman (2014), Impacts of salt marsh plants on tidal channel initiation and inheritance, *J. Geophys. Res. Earth Surf.*, 119, doi:10.1002/2013JF002900.

Received 23 JUN 2013

Accepted 19 JAN 2014

Accepted article online 28 JAN 2014

## Impacts of salt marsh plants on tidal channel initiation and inheritance

C. Schwarz<sup>1,2</sup>, Q. H. Ye<sup>3</sup>, D. van der Wal<sup>2</sup>, L. Q. Zhang<sup>1</sup>, T. Bouma<sup>2</sup>, T. Ysebaert<sup>2,4</sup>, and P. M. J. Herman<sup>2</sup>
<sup>1</sup>State Key Laboratory of Estuarine and Coastal Research, East China Normal University, Shanghai, China, <sup>2</sup>Royal Netherlands Institute for Sea Research (NIOZ-Yerseke), Yerseke, Netherlands, <sup>3</sup>Deltares, Delft, Netherlands, <sup>4</sup>Institute for Marine Resources and Ecosystem Studies, Yerseke, Netherlands

**Abstract** At the transition between mudflat and salt marsh, vegetation is traditionally regarded as a sustaining factor for previously incised mudflat channels, able to conserve the channel network via bank stabilization following plant colonization (i.e., vegetation-stabilized channel inheritance). This is in contrast to recent studies revealing vegetation as the main driver of tidal channel emergence through vegetation-induced channel erosion. We present a coupled hydrodynamic morphodynamic plant growth model to simulate plant expansion and channel formation by our model species (*Spartina alterniflora*) during a mudflat-salt marsh transition with various initial bathymetries (flat, shoal dense, shoal sparse, and deep dense channels). This simulated landscape development is then compared to remote sensing images of the Yangtze estuary, China, and the Scheldt estuary in Netherlands. Our results propose the existence of a threshold in preexisting mudflat channel depth, which favors either vegetation-stabilized channel inheritance or vegetation-induced channel erosion processes. The increase in depth of preexisting mudflat channels favors flow routing through them, consequently leaving less flow and momentum remaining for vegetation-induced channel erosion processes. This threshold channel depth will be influenced by field specific parameters such as hydrodynamics (tidal range and flow), sediment characteristics, and plant species. Hence, our study shows that the balance between vegetation-stabilized channel inheritance and vegetation-induced channel erosion depends on ecosystem properties.

## 1. Introduction

Tidal wetlands are often dissected by networks of channels shaped through tidal oscillations and their related water fluxes [Fagherazzi and Sun, 2004]. These tidal channels constitute basic pathways for the exchange of water, sediment, organic matter, organisms, nutrients, and pollutants between the wetland and the adjacent open water body [Perillo et al., 2009]. Despite the widely known relevance of tidal channels, their formation mechanisms are not well understood.

The traditional literature on tidal-channel development separates the process into two sequential stages. During the initial development, the tidal networks quickly cut through intertidal mudflats and acquire their basic structure [e.g., Allen, 2000; D'Alpaos et al., 2005; French and Stoddart, 1992] in analogy to their fluvial counterparts [e.g., Rinaldo et al., 1998]. This phase is followed by a slower elaboration phase where bank stabilization through plant colonization and meandering reinforce and elaborate the basic channel structure [Marani et al., 2002; Perillo et al., 2009; Pestrong, 1972]. The initial development phase, which is the focus of our study, starts with topography-guided sheet flows concentrating their discharge into depressions. Locally, the critical erosion threshold in bed shear stress is surpassed, leading to incision of small channels which further grow by headward erosion [Allen, 2000; D'Alpaos et al., 2007; Fagherazzi and Sun, 2004; Perillo et al., 2009]. Supported by laboratory experiments and modeling studies, this conceptualization suggests that channel network incision is mainly controlled by topography-induced water surface elevation gradients driving network expansion and shaping intertidal morphology [D'Alpaos et al., 2007; Steel and Pye, 1997; Stefanon et al., 2010; Vlaswinkel and Cantelli, 2011]. Vegetation is considered mostly as a passive agent stabilizing the banks of already incised mudflat channels. We refer to this concept as "vegetation-stabilized channel inheritance".

More recently, tidal channel development has been coupled to the effect of vegetation. Intertidal vegetation reduces flow and enhances sedimentation within vegetation patches [Bouma et al., 2007]. This flow reduction within the patches is tightly coupled with flow acceleration around the vegetation patches, where soil erosion is

initiated [Bouma *et al.*, 2009b]. Thus, the vegetation acts as an “ecosystem engineer,” i.e., as an organism able to affect biotic and abiotic properties of the environment, which can further feedback on the engineer and associated organisms [Jones *et al.*, 1994]. This stress divergence and local concentration were identified as a main factor generating spatial heterogeneity in salt marsh pioneer zones [Bouma *et al.*, 2007, 2009b; Prosser and Slade, 1994; van Wesenbeeck *et al.*, 2008]. Temmerman *et al.* [2007] modeled the consequences of these positive (promoted accretion within patches) and negative feedback (promoted erosion around patches) on intertidal landscape development. They demonstrated the ability of intertidal vegetation to actively influence channel incision by concentrating the tidal flow into narrow passages between patches. We refer to this alternative hypothesis for channel generation as “vegetation-induced channel erosion” during a mudflat-salt marsh transition.

In this paper, we argue that vegetation-stabilized channel inheritance and vegetation-induced channel erosion are both occurring in the field and that the relative importance of each depends on the physical settings of the system. We subsequently identify the specific conditions favoring either channel inheritance or channel erosion. Both aspects are studied using the modeling suite Delft3D to simulate the channel development on a mudflat in the presence of our model salt marsh pioneer species *Spartina alterniflora*. The model we use is a fully coupled hydrodynamic, morphodynamic, and vegetation model. We use this model to simulate simultaneous channel and vegetation development with and without the presence preformed mudflat channels. Finally, we test our model results with data from salt marsh ecosystems in both the Yangtze estuary (China) and the Scheldt estuary (Netherlands).

## 2. The Model

### 2.1. Model Description

We use Delft3D, developed by WL/Delft Hydraulics [Roelvink and van Banning, 1995; Wang *et al.*, 1995]. Delft3D is a finite difference numerical modeling system composed of modules describing waves, currents, sediment transport, and bottom changes, linked by a steering module (Delft3D FLOW) [Lesser *et al.*, 2004]. The Delft3D FLOW module computes tidal flow by solving the unsteady depth-averaged shallow water equations in two dimensions [Lesser *et al.*, 2004; Marciano *et al.*, 2005]. The implemented morphodynamic model is based on the advection-diffusion equation for suspended sediment transport, computing sediment transport based on time-dependent flow fields subsequently solved using semiempirical formulae. Erosion and deposition are dependent on the local flow conditions generated by the imposed water level variations at the open boundary. Changes in bathymetry due to erosion or deposition are updated by the morphodynamic model and fed back to the hydrodynamic module.

In this study we combine the 2-D depth-averaged Delft3D-FLOW module with an ecological module. The ecological module was developed within Delft3D-WAQ using an Open Process Library. The ecological module takes care of two types of processes. First, it accounts for the influence of vegetation on flow and turbulence. Vegetation stems and leaves exert an additional drag force on the flow and generate turbulence [López and García, 1998], but at the same time also reduce turbulent energy within the canopy [Leonard and Croft, 2006], thus affecting particle settling velocities [Nepf, 1999] and promoting biologically mediated sedimentation within vegetation patches [Mudd *et al.*, 2010]. This is modeled by an adapted  $k-\epsilon$  formulation explicitly accounting for the influence of rigid cylindrical plant structures on drag and turbulence [Baptist *et al.*, 2007; Uittenbogaard, 2003]. Details of the model formulation are given by Temmerman *et al.* [2007] and Baptist [2005] (Table A1). The net result of vegetation on the flow is that flow is decelerated in vegetation patches and accelerated in the immediate surroundings. This affects (through the morphodynamic model formulations) entrainment and transport of sediment, as well as local deposition processes. Second, the vegetation module simulates spatiotemporal changes in stem density and stem height of *Spartina alterniflora* [Temmerman *et al.*, 2007]. Initial plant establishment on bare grid cells is modeled stochastically with a user-defined initial plant cover and tussock diameter. Lateral expansion of plants to neighboring cells is modeled through a diffusion equation. Stem density grows up to a carrying capacity according to a logistic growth equation. Stem height growth is also modeled as logistic growth to a maximum. Stem diameter grows linearly in time, depending on stem height. Plant mortality is determined by tidal flow stress, modeled proportional to bed shear stress exerted by flow, and by inundation stress, modeled proportional to inundation height at high tide [Temmerman *et al.*, 2007]. A detailed description of the Delft3D model including the ecological module can be found in Ye [2012].

Hydrodynamic processes, such as tidal flow, and morphodynamic processes, such as suspended sediment transport and bed load transport (with bed slope effects), are used from the Delft3D-FLOW module. All processes (hydrodynamic, morphodynamic, and ecological) are considered to have mutual interactions at

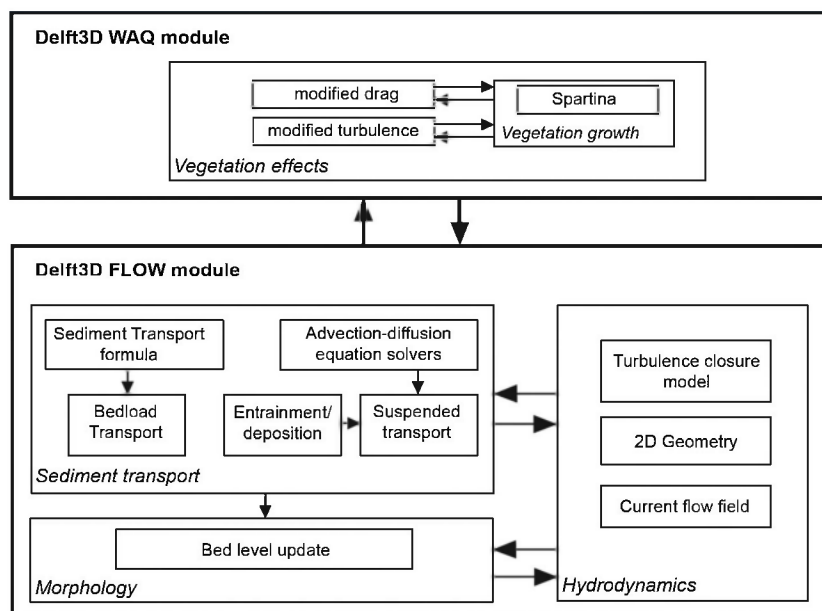


**Figure 1.** Flow diagram describing the interactions between sediment transport, morphology, hydrodynamics, and vegetation in our model simulation.

user-defined time steps. Hydrodynamic and morphodynamic processes are solved at a 2 s interval. The ecological module interacts with the hydrodynamic module updating ecological parameters at a 30 min interval. At that interval, ecological parameters such as stem height, stem diameter, and stem density are updated in the hydrodynamic and morphodynamic computations. The plant flow interactions used in this study have been extensively described and validated against flume experiments [Baptist, 2005; Bouma et al., 2007; Uittenbogaard, 2003], salt marsh field measurements [Temmerman et al., 2005], and previous modeling studies [Temmerman et al., 2007; Ye, 2012] (Figure 1).

## 2.2. Model Setup

The model uses a schematic representation of a tidal basin with a mesotidal range. It focuses on tidal currents; waves are not accounted for. A rectangular grid is used in the numerical computation in order to combine a manageable computation time with sufficient resolution of the basin morphology. The model covers an area of 1800 m × 600 m, with a grid size of 6 m and a slope of 0.1%. The highest point of the sloped platform lies at 0.2 m below the mean tidal oscillation. It is enclosed by three fixed and impermeable boundaries (closed boundaries) and one open water-level boundary at the seaward edge. It has uniform bottom sediment composed of fine sand ( $d_{50} = 80 \mu\text{m}$ ). The hypothetical mudflat elevation and slope correspond to mudflats and pioneer zone wetlands found in the Yangtze estuary, China [Schwarz et al., 2011; Yang et al., 2011; Zhu et al., 2011].

We simulate four different cases of initial mudflat bathymetries on which vegetation is added: “plain”, “shoal dense channels”, “shoal sparse channels,” and “deep dense channel”. The first simulation (“plain”) starts with a uniform bathymetry (Figure 2c, plain). This simulation runs to a dynamic equilibrium to determine the form of the spontaneously generated channel network (Figure 2d, plain). In this context a dynamic equilibrium is reached when channel network structure ceases to change, through the established equilibrium between plant regrowth and hydrodynamic-induced die-off. We use the Pearson correlation coefficient to visualize the establishment of a dynamic equilibrium (R1) and as a proxy for the self-organization of our system (R2). The Pearson product-moment correlation is a measure of linear association between two variables with a range between  $-1$  and  $+1$  [Rodgers and Nicewander, 1988]. Figure 3 shows the Pearson correlation coefficient of the bathymetry at the long-shore transect between two consecutive time steps (R1) throughout our simulation run. The establishment of the dynamic equilibrium of the channel network structure is visible by the Pearson correlation coefficient approaching 1. Note that the bathymetry keeps changing also after the coefficient has approached 1, but the changes become uniform over platform and channels, which is the reason for their lack of influence on the correlation coefficient. Subsequently, artificial channel networks based on this blueprint, but originating from a

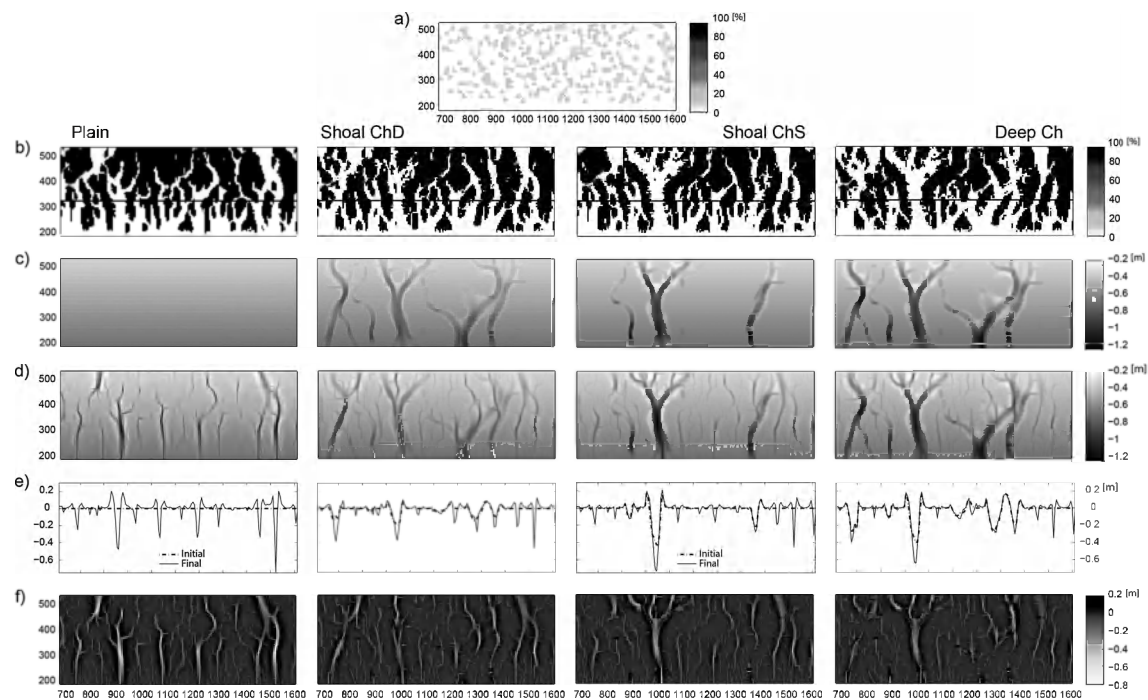


**Figure 2.** Plan view of the modeling results for the four initial bathymetries used in this study (flat bathymetry (plain), shoal imposed channels with high density (shoal dense channels; Shoal ChD), shoal imposed channels with low density (shoal sparse channels; Shoal ChS), and deep imposed channels with high density (deep dense channels; Deep Ch)). (a) The configuration of the initial plant cover and (b) the plant cover after 3 years is shown as a percentage of the maximum stem density. (c) The morphologic evolution from initial bed level to (d) the bed level after 3 years is shown through the platform elevation in meters. (e) A comparison between the initial and final bed configuration is shown across a long-shore transect, indicated by the black line in Figure 2b. (f) The sediment movement throughout our simulation is shown through the cumulative change in sedimentation/erosion after 3 years in meters.

different initial random plant pattern, are imposed onto the model domain before introduction of the vegetation (Figure 2c, Shoal ChD, Shoal ChS, Deep Ch). This is done in different ways. In the “shoal dense channels” case (Shoal ChD) the full network topology of channels is used, but the depth relative to the platform is reduced by 50% compared to the dynamic equilibrium network (maximum depth relative to the platform equal to 0.35 m, number of induced channels equal to 5). In the “shoal sparse channels” case (Shoal ChS) the number of main channel branches is reduced from 5 to 3, but the total initial channel volume is the same as in the “shoal dense channel” case. Consequently, the channels are deeper than in that case (i.e., maximum depth relative to the platform equal to 0.6 m, number of induced channels equal to 3). Finally, in the “deep dense channels” case (Deep Ch) the dynamic equilibrium channel network is used at full extent in the initial conditions (i.e., maximum depth relative to the platform equal to 0.7 m, number of induced channels equal to 5).

Tidal action is simulated by applying a sinusoidal water-level fluctuation at the open boundary (amplitude = 1.2 m), where also an equilibrium sediment concentration is assumed. The equilibrium sediment concentration which is calculated over the vertical profile of the suspended transport varies over space and time and depends on the bed shear stress and water depth [van Rijn, 1993, equation (9.3.4)]. It is numerically implemented by setting the sediment concentration gradient at the boundary to zero when solving the transport equations. Tidal range and sediment concentration correspond to actual field situations found in pioneer zone salt marshes in the Yangtze estuary. To overcome the issue related to differences in time scales over which hydrodynamic and morphodynamic processes occur, a morphological factor accelerating morphological change by extrapolating the bathymetric changes was utilized [Marciano *et al.*, 2005]. The model simulates an average sidereal month (27 days) which is then upscaled using a morphologic factor (24) to an overall time of 3 vegetation periods (8 months vegetation period per year; 24 months = 3 vegetation periods, i.e., 3 years). The morphological factor is implemented by multiplying the erosion and deposition fluxes from the bed to the flow and vice versa by an integer number at each computational time step. This allows accelerated bed-level changes to be incorporated dynamically into the hydrodynamic flow calculations. The morphological factor is chosen to be 24, since from a hydrodynamic point of view this increase in morphological development does not crucially influence hydrodynamics and allows us to extrapolate our simulation

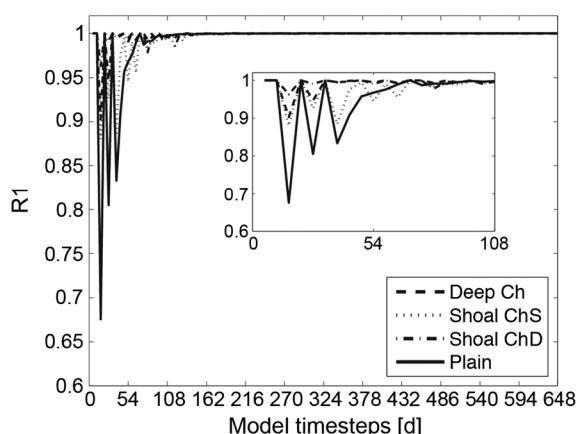


**Figure 3.** The Pearson correlation coefficients ( $R1$ ) between consecutive time steps of the long-shore bathymetry plotted over simulation time [d] is shown. The establishment of a dynamic equilibrium after  $n$  model time steps is visible through the line advancing toward one. The inset shows the magnified area from model time steps 0 to 108 days.

results to a 3 year period. Hydrodynamic processes are updated every 2 s; including the morphological factor, this gives an update rate of every 48 s. The ecological module interacts with the hydrodynamic module every 30 min, which denotes an update of vegetation metrics every 12 h, producing enough temporary resolution to allow interactions between vegetation growth, hydrodynamics, and sediment dynamics.

Statistical properties of the initial plant cover are derived from multiple remote sensing images of the pioneer zone of the *Spartina alterniflora* marsh at the beginning of the growing season in the Yangtze estuary, China. In these images, the average plant cover is 25% with an average tussock diameter of 18.3 m. Based on these observations, the initial plant cover in our modeling domain is realized as a random pattern of tussocks with a diameter of 18 m and overall area coverage of 25%. Initial plant density within tussocks ( $80 \text{ stems m}^{-2}$ ) and initial plant height (0.17 m) at the starting point of our simulations are set at 10% of the maximum density ( $800 \text{ stems m}^{-2}$ ) and height (1.7 m), respectively (Table A2).

Simulations show that the chosen time frame (three vegetation periods) is sufficient for plant growth, hydrodynamics and sediment transport to reach a dynamic equilibrium (see Figure 3).

### 2.2.1. Model Analysis

A region in the center of the modeling domain at which the influence of the closed boundaries is negligible was determined as the result of our modeling computation (Figure 4). Since closed boundaries in combination with adjacent vegetation can also act as flow routing agents leading to channel incision, we exclude the closed boundary adjacent areas from our analysis. In this area a long-shore profile is drawn at the location of maximum longitudinally averaged erosion (see the grey shore-parallel plane in Figure 4 and the black horizontal line in Figure 2b). The location of maximum longitudinally averaged erosion, which is determined from the model output, is dependent on the occurrence of maxima in bottom shear stresses, which are determined by the slope, platform elevation, water level, current velocity, and sediment properties. The location of the maximum longitudinally averaged erosion is subject to changes throughout the morphological evolution of the salt marsh; nevertheless, in due course it establishes dynamic equilibria which we use for our model and field comparisons. At the location of this long-shore profile we calculate the cross-sectional projected plant area and the cross-sectional eroded channel area (Figures 4 and 2b).

We calculate the cross-sectional projected plant area ( $\text{m}^2$ ) at the long-shore profile by multiplying the plant height (model output) until the water height of maximum sediment transport (i.e., 0.4 m above bed) by the length of our long-shore profile (Figure 4). The cross-sectional projected plant area is calculated at two instances: (1) at the beginning (after the initial pattern established a temporal equilibrium with sediment transport; initial pattern, see also Figure 2a) and (2) at the end of our model simulation (see also Figure 2b). The cross-sectional eroded channel area ( $\text{m}^2$ ) along our long-shore profile is also calculated at these two time points.

We use the Pearson correlation coefficient to calculate how well the bathymetry along the long-shore transect remains correlated with the initial bathymetry over the course of our simulation (further referred to as  $R2$ ).



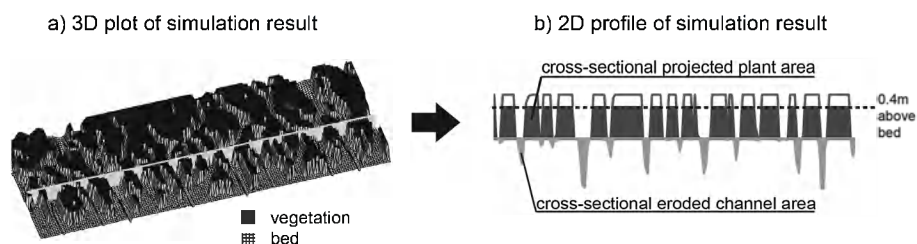


**Figure 4.** Schematic representation of the model analysis. (a) A 3-D plot of the model domain shows vegetation (black) and the bed with its eroded channels (grey). The light grey long-shore plane represents the wet cross-sectional area at the location of maximum longitudinally averaged channel erosion, with its height indicating the water level of maximum sediment transport (0.4 m above bed). (b) The 2-D profile at the location of the long-shore plane, with its projected cross-sectional plant area and the cross-sectional eroded channel area is shown.

A drop in Pearson product-moment correlation to zero, i.e., the current bathymetry becoming independent from the initial one is interpreted as an indication for self-organization. Low values in the Pearson correlation coefficient indicate significant changes in bathymetry, whereas high-correlation values denote little or relative changes in bathymetry, such as channel deepening. The ability to alter the habitat independent of its initial state is a characteristic of a self-organized system. In this context self-organization denotes the ability of organisms (through local feedback) to physically alter their environment producing spatial heterogeneity (Figure 5d) [Rietkerk *et al.*, 2002; van de Koppel *et al.*, 2005].

#### 2.2.2. Testing

Our model results are qualitatively tested through comparison with a time series of digitized aerial photographs (2003) and Quickbird satellite images (2005) of an expanding *Spartina alterniflora* salt marsh located on Chongming Island (Yangtze estuary, China) (Figure 7). We specifically identify the emergence of salt marsh channels at a mudflat-salt marsh transition, at locations with and without preexisting mudflat channels. This is compared with the emergence of tidal channels with and without preexisting mudflat channels of our model simulations.

In addition, we compare our model output to an expanding salt marsh located in the Southwest delta of Netherlands (Walsoorden tidal flat in the Westerschelde estuary, 51.4°N, 4.1°E) (Figure 8). On this tidal flat, a salt marsh started developing in the late 1990s as isolated clumps of plants, mostly *Spartina anglica*, *Salicornia procumbens*, and *Aster tripolium*. van der Wal and Herman [2012] and van der Wal *et al.* [2008] give the results of detailed field studies of this development. We make use of aerial photographs, digital elevation models, and water level measurements in 2004 and 2008 as a basis of our calculations. Water level data is interpolated from two adjacent tide gauge stations Hansweert and Bath (<http://live.getij.nl>). The data shows high conformance with field measurements at our research sites. DEM (digital elevation model) data is obtained from airborne laser altimetry (lidar) surveys provided by Rijkswaterstaat, with 2 m spatial resolution [van der Wal and Herman, 2012]. Cross-referenced in situ dGPS (differential Global Positioning System) assays at our investigated site

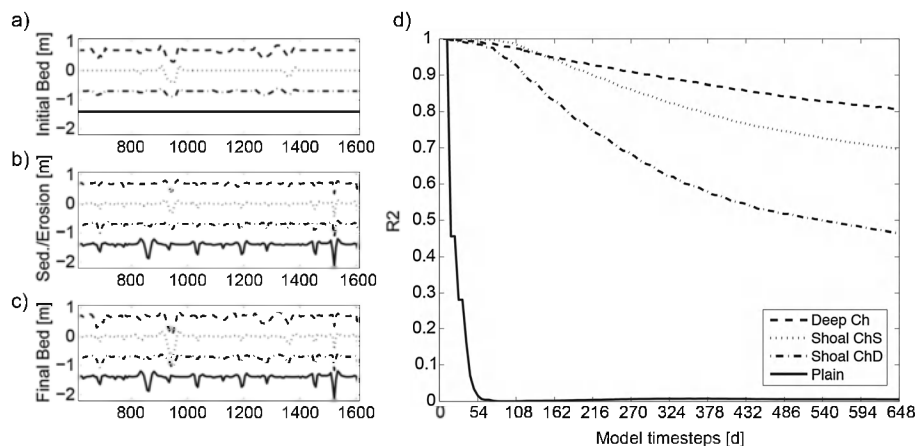


**Figure 5.** Comparison of eroded channels along the long-shore transect. We compared (a) the initial bed levels, (b) the cumulative sedimentation/erosion at the end of our simulation, and (c) the final bed level (scaled for 1:1 comparison). (d) We further show the change in bed morphology by calculating Pearson correlation coefficients ( $R^2$ ) between the initial long-shore bathymetry and long-shore bathymetry after  $n$  model time steps [d].

confirm the DEM's accuracy. Plant height data of the mixed community (*Spartina anglica*, *Salicornia procumbens*, and *Aster tripolium*) is based on field assays and literature (average plant height: 0.7 m) [van der Wal and Herman, 2012; van der Wal et al., 2008]. We fix a long-shore profile in the developing marsh at the location in the cross-shore direction where channel incision is maximally developed according to the DEM. We determined the water height at the tidal phase when current velocity and hence sediment erosion was maximal (0.5 m above Normaal Amsterdams Peil (NAP), the Dutch Ordnance Level) using field measurements. The distribution of plants along our long-shore transect is assessed by calculating the NDVI (normalized difference vegetation index) of geocorrected false color aerial images using digital numbers (DNs) in the red (R) and near-infrared (NIR) according to  $NDVI = (DN_{NIR} - DN_R) / (DN_{NIR} + DN_R)$  and setting a threshold NDVI to discriminate between vegetation and bare tidal flat. The aerial photographs are provided by Rijkswaterstaat and have a spatial resolution of 25 cm [van der Wal et al., 2008]. Based on these measurements in 2004 and 2008, we calculate changes in the cross-sectional projected area of plant stands and in the cross-sectional area of eroded channels in this 4 year period.

### 3. Results

The simulations start from a homogeneous flow field without vegetation. After imposing the random starting configuration (based on field data), flow is obstructed by the vegetation patches and is deflected to the immediate vicinity of the patches, where velocity and bed shear stress increase. Due to plant growth and thus increase of the density, height, and lateral extension of the patches, this effect increases through time. When the bed shear stress in between patches surpasses the critical threshold for sediment movement, tidal channels are initiated. In turn, the high flow and bed shear stress in the channels inhibit further lateral development of the vegetation and fix the channel. Through the pronounced levee alongside the eroded channels (Figures 2 and 5), it emerges that eroded sediments accumulate within the vegetated area. During this phase of self-organization of the landscape, not all gaps between vegetation patches develop into channels. In many places the current velocities do not surpass the critical threshold and the patches merge to form the vegetated marsh platform. Channels are formed at more or less regular intervals in space (Figures 2b–2f, plain).

The cases with preformed channels present before the start of the simulation show a different pattern (Figure 2, Shoal ChD, Shoal ChS, Deep Ch). The influence of vegetation on the resulting channel pattern is dependent on how well-formed the channels are before development starts. At shoal mudflat channels, although erosion within the channels is promoted, there is enough momentum left for channel erosion through plant-flow interactions. This results in a new equilibrium for emerging channel networks and vegetation patch arrangement (Figures 2b–2f, Shoal ChD). In the case where the number of channels is reduced but the total channel volume is kept exactly equal, erosion is even more concentrated in the channels and less pronounced in the adjacent areas. The channels in this case are deeper than in the Shoal ChD case, and this apparently attracts flow and erosion to further concentrate in these places (Figure 2b–2f, Shoal ChS). When the imposed mudflat channels are even deeper and the network is fully extended (Deep Ch), the above-described impacts (i.e., deepening of preexisting incised channels, reduction of new channels formed by plant-flow interactions) get more pronounced (Figures 2b–2f, Deep Ch, and Figures 5a–5c).

We then calculate how well the bathymetry along the long-shore transect remains correlated with the initial bathymetry. This reveals that in the plain scenario all correlation with the initial bathymetry is quickly lost (Figure 5d), which can be interpreted as a sign that the landscape is self-organizing without memory of its previous state. In the cases where channels are preimposed onto the landscape, the correlation decreases over time due to more restricted self-organization (by preimposed channels), but there always remains a considerable correlation with the initial bathymetry. The deeper the imposed channels are, the more the bathymetry remains correlated with the initial state over time, showing that self-organization is limited and the imprinted morphology is largely retained. The fact that lines in Figure 5d seem not to flatten is due to the fact that the channel network bed is still experiencing differential sediment transport compared to the platform influenced by the morphologic factor. The difference between plain and imposed mudflat channels also becomes visible through a comparison of the channel spacing between the different scenarios. Average channel spacing was  $34.59 \text{ m} \pm 3.97$  in the plain scenario,  $43.84 \text{ m} \pm 4.82$  in shoal dense channels scenario,  $43.29 \text{ m} \pm 3.46$  in the shoal sparse channels scenario, and  $47 \text{ m} \pm 3.37$  in the deep dense channels scenario (Figure 2).

A comparison between the cross-sectional projected plant area, cross-sectional eroded channel area, and the cross-sectional imposed channel area along the long-shore transect (Figure 6) reveals that with homogenous initial bathymetry (i.e., without preimposed channels) the change between cross-sectional eroded channel area is

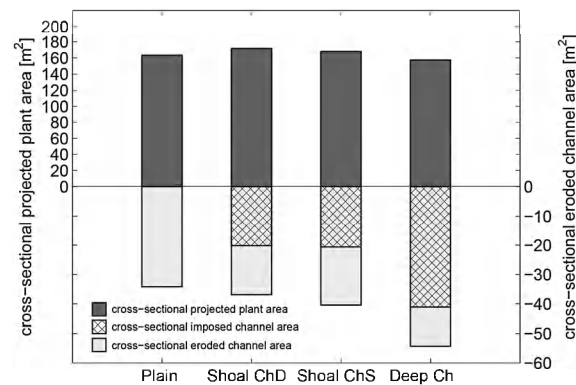


**Figure 6.** Comparison between the cross-sectional projected plant area (dark gray), with the cross-sectional eroded channel area (light gray) in combination with the cross-sectional imposed channel area (hatched) at the end of our model simulation.

clearly related to the change in cross-sectional projected plant area (the ratio between the relative increase in cross-sectional projected plant area to relative increase in channel area is  $4.1:4.4 = 0.93$ ) (Figure 6, plain). This ratio is relative to the cross-sectional eroded channel area and the cross-sectional projected plant area of the established temporal equilibrium in sediment transport at the initial plant pattern. The fact that the cross-sectional area of eroded channels matches the increase of cross-sectional projected plant area implies that these channels are generated solely by plant-flow interactions. As soon as mudflat channels are imposed (i.e., preimposed cross-sectional-imposed channel area increases), the cross-sectional eroded channel area decreases significantly, decoupling the relationship between the increase cross-sectional projected plant area and the newly eroded cross-sectional eroded channel area. The deeper the preimposed channels get, the smaller the influence of the cross-sectional projected plant area on the resulting bed configuration seems to become (Figure 6, Shoal ChD, Shoal ChS, and Deep Ch). This is also visible in the comparison of the relative increase in cross-sectional projected plant area: relative increase channel area, for Shoal ChD, Shoal ChS, and Deep Ch, which gives  $4.2:2.7 = 1.55$ ,  $4.2:2.7 = 1.55$ , and  $3.9:1.7 = 2.29$ , respectively. The slight increase in cross-sectional projected plant area from plain to shoal channels dense (Shoal ChD) in Figure 6 is a function of the higher drainage density of the incised channels in the plain case.

### 3.1. Field Comparison (China)

Comparing a digitized aerial photograph from January 2003 (Figure 7a) with a Quickbird image from November 2005 (Figure 7b) shows the rapid expansion of the *Spartina alterniflora* pioneer vegetation on Chongming Island (Yangtze estuary, China). The pictures are taken outside of the season when the pioneer zone expands, thus showing the closed marsh vegetation versus the bare mudflat areas. The dense *Spartina* vegetation is clearly intersected by tidal channel systems, which discharge into mudflat channels. Compared to 2003, the salt marsh has expanded over a distance of about 700 m in 2005. In this process, the former mudflat/pioneer zone was transformed into a dense-colonized meadow dissected by channels. This process is also reproduced in our simulation, where a mudflat colonized with scattered vegetation patches (Figure 2a) develops into a vegetated

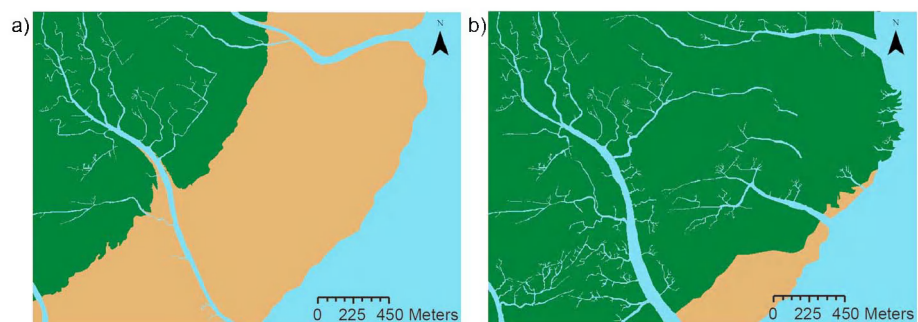


**Figure 7.** Digitized aerial photographs showing a vegetated marsh (green), mudflat (brown) with its adjacent water body, and tidal channels (blue) on Chongming Island, Yangtze estuary, China. The salt marsh expansion and channel development from (a) 2003 to (b) 2005 is shown.



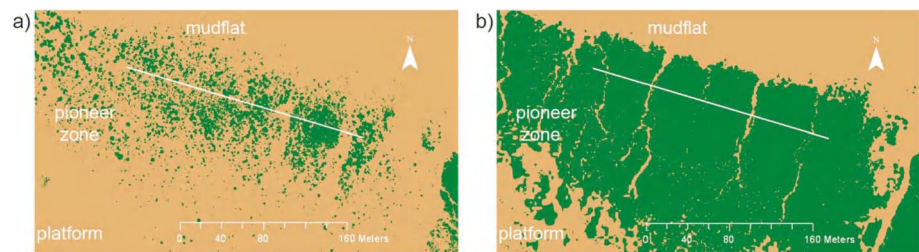


**Figure 8.** Digitized aerial photographs showing the salt marsh expansion (green) and channel development on a bare mudflat (brown) at Walsoorden, Scheldt estuary, Netherlands. The development from (a) 2004 to (b) 2008 is shown.

meadow dissected by intertidal channels (Figure 2b, plain). The comparison of these two photographs shows on the one hand the inheritance of preexisting mudflat channels in the salt marsh channel network, while on the other hand, it shows the incision of new mudflat/salt marsh channels after vegetation encroachment took place. We propose that the newly incised channels originate from vegetation-induced channel erosion processes (channels located between the former mudflat channels). It cannot be excluded that mudflat channels were formed before the vegetation encroached the platform at our Chinese field site, but the smoothness of the mudflat as observed in the field strongly suggests that vegetation-induced channel incision is more important than topography-induced channel incision in this case. This corresponds qualitatively with the predictions from our model and suggests that some salt marsh channels originate from plant-flow interactions whereas others from stabilizing characteristics of vegetation inheriting existing mudflat channels.

### 3.2. Field Comparison (Netherlands)

In 2004, on a mudflat with recently established vegetation patches (characterized by *Salicornia procumbens* and *Aster tripolium* [van der Wal and Herman, 2012]) (Figure 8a), channel initiation was not yet visible from the aerial photograph, as was also confirmed by little variation in initial bathymetry. In fact, at this time the variation in bathymetry is within the uncertainty range of laser altimetry. By 2008 the vegetation patches had expanded laterally, forming a dense meadow intersected by tidal channels (Figure 8b). Our model reproduces this observed pattern of plant expansion and channel initiation very well. Channels in our simulation are well developed. Comparing the cross-sectional projected plant area with the cross-sectional eroded channel area along a long-shore transect through the zone of maximal channel incision (white line in Figure 8) at the two time points reveals a close correspondence in the relationship between the measured (Figure 9b) and modeled (Figure 6, plain) ratio between the relative increase in cross-sectional areas (increase in cross-sectional projected plant area to increase in channel area, field comparison:  $1.9:2.1 = 0.90$ , plain:  $4.1:4.4 = 0.93$ ). In both cases it is visible that the increase in eroded channel area is due to an increase in cross-sectional projected plant area. The increase of eroded channel area will depend on vegetation cover, hydrodynamic conditions, and sediment properties.

## 4. Discussion

Previous studies have highlighted the influence of vegetation on flow [e.g., Hickin, 1984; Nepf, 1999, 2012; Vandenbruwaene et al., 2011], local sediment transport [e.g., Bouma et al., 2009b; van Wesenbeeck et al., 2008], and channel incision [e.g., Temmerman et al., 2007]. The present study extends the previous knowledge by linking initial bathymetry to plant-flow interactions. Our model results confirm the influence that plants may exert on the

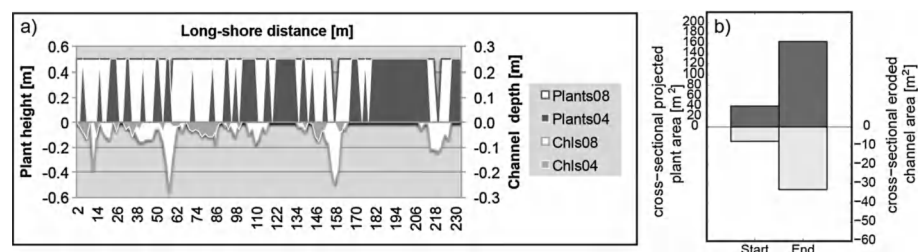


**Figure 9.** (a) Long-shore profile at Walsoorden in 2004 and 2008 at its maximum erosion zone (see also white line Figure 7). (b) A comparison between the cross-sectional projected plant area (dark gray) and the cross-sectional eroded channel area (light gray) along the long shore profile at this two time points (2004 and 2008).

formation of channels, as previously shown by *Temmerman et al.* [2007]. However, we also show that the degree to which these interactions determine the final landscape depends strongly on the configuration of the landscape at the stage when plant colonization takes place. The absence or presence of preexisting mudflat channels will determine whether enough momentum is present in the flow field outside the preformed channels to incise new ones. Moreover, the ability of preexisting channels to redistribute momentum between channels and the unchanneled vegetated platform depends on the platform elevation relative to the mean sea level. Our results show that the ratio between overland flow and channel flow during a tidal cycle, which is dictated by the platform elevation relative to the tidal frame, exerts a strong influence on emerging channel network drainage density [*van Maanen et al.*, 2013; *Vandenbruwaene et al.*, 2012]. Our model results also indicate that in cases where channels attract most of the flow, additional erosion is likely to occur within the preformed channels, rather than as extension of the channel network. These results are in agreement with *Temmerman et al.* [2007], who expressed the expectation that plant-flow interactions are most important in landscapes with rather homogeneous gradients in topography and soil conditions (further referred to as “excess momentum” concept). They are also applicable to vegetation-stabilization observed in alluvial systems [*Gran and Paola*, 2001].

From the comparison of our modeling results with field observations, it appears that the balance between erosional and stabilizing vegetation properties is strongly linked to the presence or absence of halophyte vegetation during the short time span in which tidal channel incision takes place. In the absence of vegetation during this incision phase, vegetation is more likely to fulfill a stabilizing function on already incised mudflat channels [*D'Alpaos et al.*, 2005]. With vegetation present during the channel incision phase, a mixture between erosional and stabilizing properties of vegetation (linked to mudflat topography) can be expected, as shown on our research area in China and in the Netherlands. In this case the predominance of erosional or stabilizing properties will depend on the interaction between hydrodynamics, sediment, and plant properties [*Gao et al.*, 2011; *Temmerman et al.*, 2007; *van der Wal and Herman*, 2012; *Xu and Zhuo*, 1985].

Our simulations suggest through the decoupling of the cross-sectional projected plant area and the cross-sectional eroded channel area that channel inheritance is the dominant mechanism on mudflats with a preexisting deeply incised channels rendering the influence of vegetation-induced channel erosion as insignificant. This proposes a threshold in mudflat channel depth favoring either channel inheritance or new channel incision. In this context, what is “deep” and “shoal” is a relative measure. In our study we refer it to the maximum depth in a channel system entirely produced by vegetation-induced self-organization, but in field studies this depth is unknown. It will be determined by field-specific characteristics such as hydrodynamics (tidal range, waves, and flow), sediments, and predominant plant species. The predominance of either inheritance or erosion depends on the significance of plant-flow routing compared to flow routing by mudflat topography. It was previously shown that different hydraulic resistance of plants (produced through, e.g., stiffness) is able to influence the magnitude of their flow retardation and diversion [*Bouma et al.*, 2009a]. This insight has further repercussions in the light of our model results. For instance, on a topographically heterogeneous mudflat colonized by vegetation with low hydraulic resistance, flow retarded and diverted by vegetation patches might be insufficient to cause channel erosion. In this scenario topography-guided erosion will be predominant allowing vegetation to colonize areas between incised mudflat channels and hence stabilize them. If the same mudflat is colonized by vegetation with high hydraulic resistance, the magnitude of plant-flow interactions might be sufficient to cause channel erosion, rendering it predominant over topography-guided erosion.

Our process-based model shows channel initiation, through erosive processes caused by flow routing, leading local bottom shear stress to exceed the threshold for initiating sediment motion. This threshold, in literature also referred to as critical bed shear stress, is a function of the median sediment grain size ( $d_{50}$ ) and was calculated according to *van Rijn* [1993, equation (4.1.11)]. The importance of erosive processes for channel initiation assumes that channel development can be separated in two different processes: a fast initial erosive phase followed by a slower phase of network elaboration (including processes as meandering). Previous literature justifies this separation into two development stages by showing the importance of headward erosion and the insignificance of meandering processes at initial creek formation [*French and Stoddart*, 1992; *Gabet*, 1998; *Pestrong*, 1965; *Steers*, 1960]. In fact, most studies on channel formation stress the importance of erosion processes, although some previous studies also found depositional processes guiding tidal channel emergence. Literature revealed that the formation of narrow marsh channels originates from differential sediment deposition within vegetation patches which lead the vegetated platform to constrict already-existing dynamic mudflat

channels, hence inheriting them [Redfield, 1965; Steers, 1960]. This was also documented by deposition-guided channel emergence, originating from the coalescence of Marsh Islands during delta progradation [Hood, 2006]. The basic processes needed for these depositional channel modifications are incorporated into our model: enhanced sedimentation inside vegetation patches and coalescence of laterally expanding patches without channel formation in between. Thus, our model implicitly also represents this mechanism. Based on our model and existing literature, we suggest that erosion at vegetation edges and differential deposition within them are two mechanisms always present. The classification in erosional or depositional channel emergence merely depends on the predominance of one process or the other. We suggest that the predominance of one process will depend on local factors such as sediment characteristics (cohesive and noncohesive), suspended sediment concentrations, hydrodynamic conditions (currents and waves), and plant properties (hydraulic resistance and density height). This would also give a possible explanation for the different predictions on the influence of vegetation on channel density by Kirwan and Murray [2007] and Temmerman *et al.* [2007].

Our model does not explicitly account for soil and bank stabilization by plant roots. Nevertheless, it indirectly accounts for this stabilizing plant property by the interactions of the aboveground structures on local drag and turbulence and the resulting hampered sediment erodibility adjacent to vegetation stems. One constraint of our simulation is the prohibition of erosion at wet-dry cell interfaces (e.g., bank erosion during channel filling), since the model only accounts for erosion of wet cells. This probably leads to an overrepresentation of channel bed erosion and bank stabilization and an underrepresentation of bank erosion. However, since our simulation is intended to mainly simulate the initial channel development phase, these processes are of less importance, compared to the subsequent elaboration phase (characterized by processes such as channel meandering).

We do not include seedling establishment in our simulation since starting from an established plant pattern (based upon our field situation), an additive number of random seeding by seedlings would not affect the resulting patterns significantly. Our simulation starts from a random organization of plant patches in which statistical properties such as density, coverage, height, and diameter of the plants were chosen according to the field situation (field measurements and aerial images). This is due to the fact that the seedlings possess a lower stress tolerance than existing tussocks and are therefore unable to occupy bare spots which can be occupied by lateral tussock growth.

We are aware that our model depicts an oversimplification and is therefore not able to completely explain the field scenarios (Figures 7 and 8). A major difference is caused by sediment composition. Sediment characteristics (e.g., cohesive versus noncohesive) are the determining factors for critical bottom shear stress thresholds of sediment erosion and therefore channel initiation [van Ledden *et al.*, 2004]. This impacts the probability of mudflat channel existence on the one hand and also the amount of force necessary to initiate channels via plant-flow interactions on the other hand. Further, our simulation does not include wave effects, which can also have a big impact on intertidal sediment transport [Callaghan *et al.*, 2010; Defina *et al.*, 2007]. Nevertheless, our simple hypothetical mudflat model is able to reproduce the main aspects of tidal channel initiation and inheritance in the field comparisons, giving new insights on ramifications of local vegetation properties on landscape evolution.

The concept of “excess momentum”, i.e., platform (unchanneled) flow, which interacts with aboveground vegetation structures and its potential to initiate channels, could be practically used in landscape restoration such as reforestation or wetland rehabilitation. Plant-flow interactions could be optimized in relation to initial topography, hydrodynamics, and sediment properties resulting in increased channel drainage density promoting spatial heterogeneity. Furthermore, this concept can be applied to the observed vegetation-assisted establishment of dynamic single-thread channels in stream ecosystems. In stream ecosystems it was observed that vegetation has the ability to reorganize flow patterns through bank stabilization and subsequently convert the platform morphology from braided to single thread [Tal and Paola, 2007].

## 5. Conclusions

We have shown that initial tidal channel development at constant hydrodynamic conditions is dependent on the interplay between aboveground vegetation structures and mudflat heterogeneity. Our simulations demonstrate that at homogenous mudflat bathymetry, channels are mainly formed through plant-flow interactions. The more heterogeneous the mudflat becomes, i.e., through the presence of existing mudflat channels, the smaller the influence of plant-flow interactions on the resulting landscape configuration becomes. We refer to these two concepts as vegetation-induced channel erosion versus vegetation-stabilized channel inheritance processes. Our results further

suggest that these two mechanisms are always present; the predominance of one over the other depends on the environmental conditions such as sediment properties and concentration, hydrodynamics, and plant characteristics.

Our model was able to qualitatively represent channel development in Chinese salt marshes, as well as in the widely different marshes in the Dutch field comparison. This suggests the wide applicability of our results. Future research could investigate the validity of the predictions beyond salt marsh ecosystems. Channel development in mangrove and sea grass ecosystems might also be sensitive to initial bathymetry.

Since we did not aim to create a complete landscape model but rather utilized this simple set up to investigate interactions between abiotic and biotic processes at different landscape morphologies, our approach provides the opportunity to test the ramifications of various environmental settings on landscape development. Future challenges will involve the incorporation of further biotic (such as different plant species, species competition, and the presences of different benthic organisms) and abiotic parameters (such as different suspended sediment concentrations, different mixtures of suspended and bottom sediment, and the occurrence of waves) to investigate their role in driving landscape development under various environmental conditions. This provides a unique opportunity to investigate the impact of biota on landscape development and to identify circumstances pronouncing or concealing biotic impact on the resulting geomorphology. Such dynamic view of the development of vegetated landscapes may provide the insights needed to identify the signatures of life on the landscape [Dietrich and Perron, 2006].

## Appendix A

Summary of the model equations describing the plant-flow-morphology interactions in our model simulations. Table A1 shows the model equations for hydrodynamic, morphodynamic, and ecologic processes. Table A2 explains the model parameters and used input values of the model equations in Table A1.

**Table A1.** Model Equations<sup>a</sup>

Number	Equation	Short Description
<i>Hydrodynamic Model Equations: Plant Influence on Drag and Turbulence</i>		
1	$F(z) = \frac{1}{2} \rho_0 \phi(z) n(z)  u(z)  u(z)$	Extra source term of friction force caused by plants
2	$\left(\frac{\partial k}{\partial t}\right)_{\text{plants}} = \frac{1}{1-A_p(z)} \frac{\partial}{\partial z} \left\{ (1-A_p(z)) (v + v_T / \sigma_k) \frac{\partial k}{\partial z} \right\} + T(z)$	Extra source term of turbulent kinetic energy caused by plants
3	$A_p(z) = (\pi/4) \cdot \phi^2(z) \cdot n(z)$	Table A2.
4	$T(z) = F(z) u(z) / \rho_0$	Table A2.
5	$\left(\frac{\partial \epsilon}{\partial t}\right)_{\text{plants}} = \frac{1}{1-A_p(z)} \frac{\partial}{\partial z} \left\{ (1-A_p(z)) (v + v_T / \sigma_\epsilon) \frac{\partial \epsilon}{\partial z} \right\} + T(z) \tau_\epsilon^{-1}$	Extras source term of turbulent energy dissipation caused by plants
6	$\tau_{\text{free}} = \frac{1}{c_{2\epsilon}} \left( \frac{k}{\epsilon} \right)$	Table A2.
7	$\tau_{\text{veg}} = \frac{1}{c_{2\epsilon} \sqrt{c_\mu}} \left( \frac{k^2}{\epsilon} \right)^{1/3}$	Table A2.
8	$L(z) = C_l \left\{ \frac{1-A_p(z)}{n(z)} \right\}^{\frac{1}{2}}$	Table A2.
<i>Morphodynamic Model Equations</i>		
9	$\frac{\partial c}{\partial t} + \frac{\partial uc}{\partial x} + \frac{\partial vc}{\partial y} + \frac{\partial (w - w_s) c}{\partial z} + \frac{\partial}{\partial x} \left( \epsilon_{s,x} \frac{\partial c}{\partial x} \right) - \frac{\partial}{\partial y} \left( \epsilon_{s,y} \frac{\partial c}{\partial y} \right) - \frac{\partial}{\partial z} \left( \epsilon_{s,z} \frac{\partial c}{\partial z} \right) = E - D$	Advection-diffusion equation for suspended sediment transport
10	$-w_s c - \epsilon_{s,z} \frac{\partial c}{\partial z} = 0 \quad \text{at } z = \zeta$	Water surface boundary, $z = \zeta$ equals the location of the free surface
11	$-w_s c - \epsilon_{s,z} \frac{\partial c}{\partial z} = E - D \quad \text{at } z = z_b$	Bed boundary
12	$E = \alpha_2 C_a \left( \frac{\epsilon_s}{\Delta z} \right)$	Erosion of sediment
	$D = \left[ \alpha_2 \left( \frac{\epsilon_s}{\Delta z} \right) + \alpha_1 w_s \right] c_{\text{limx}}$	Deposition of sediment

**Table A1.** (continued)

Number	Equation	Short Description
13	$q_{s,x} = \int_{z_a}^{\zeta} \left( uc - \epsilon_{s,x} \frac{\partial C}{\partial x} \right) dz$	Suspended sediment transport flux
14	$q_{s,y} = \int_{z_a}^{\zeta} \left( vc - \epsilon_{s,y} \frac{\partial C}{\partial y} \right) dz$	
14	$\frac{\partial \zeta}{\partial t} \rho_s + \frac{1}{1-p} \left( \frac{\partial q_x}{\partial x} + \frac{\partial q_y}{\partial y} \right) = S$	Bed elevation change as a result of the overall sediment transport
<i>Ecological Model Equations</i>		
15	$\frac{\partial n}{\partial t} = p_{\text{est}} + p_{\text{diff}} + p_{\text{lat,growth}} - p_{\text{flow}} - p_{\text{inu}}$	Temporal change in stem density
16	$p_{\text{diff}} = D \left( \frac{\partial^2 n}{\partial x^2} + \frac{\partial^2 n}{\partial y^2} \right)$	Lateral expansion of plants to neighboring cells
17	$p_{\text{lat,growth}} = r_1 \left( 1 - \frac{n}{K_1} \right) n$	Logistic growth of stem density up to carrying capacity
18	$p_{\text{vert,growth}} = r_2 \left( 1 - \frac{h_b}{K_2} \right) h_b$	Logistic growth of stem height up to carrying capacity
19	$p_{\text{flow}} = PE_r (\tau - \tau_{cr,p})$	Plant mortality caused by flow
20	$p_{\text{inu}} = PE_H (H - H_{cr,p})$	Plant mortality caused by inundation stress
21	$\varphi(t) = \varphi_{\text{min}} + at$	Linear increase of plant diameter

<sup>a</sup>Summary of model equations including short description (parameters are explained in Table A2).

**Table A2.** Model Parameters<sup>a</sup>

Symbol	Parameter	Unit	Value	Ref.
$x, y, z$	coordinates of grid cell	m		
$t$	time	s		
$u, v, w$	flow velocity in $x, y, z$ direction	$\text{m s}^{-1}$	M	
$F$	friction force exerted by cylindrical plant structures on the flowing fluid	$\text{N m}^{-3}$	equation (1)	
$\rho_0$	fluid density	$\text{kg m}^{-3}$	$10^3$	
$\varphi$	stem diameter of plant structure	m	equation (21)	
$\varphi_{\text{max}}$	maximum stem diameter of plant structure	m	0.01	1
$\varphi_{\text{min}}$	Initial stem diameter of plant structure	m	0.005	1
$n$	stem density of plant structures	$\text{m}^{-2}$	equation (15)	
$A_p$	horizontal cross-sectional plant area per unit area	—	equation (3)	
$k$	turbulent kinetic energy	$\text{m}^2 \text{s}^{-2}$	equation (2)	
$\epsilon$	turbulent energy dissipation	$\text{m}^2 \text{s}^{-3}$	equation (5)	
$\nu$	kinematic fluid viscosity	$\text{m}^2 \text{s}^{-1}$	$10^{-6}$	2
$\nu_T$	eddy viscosity	$\text{m}^2 \text{s}^{-1}$	$5.10^{-4}$	2
$T$	work spent by the fluid	$\text{m}^2 \text{s}^{-3}$	equation (4)	
$\sigma_k$	turbulent Prandtl-Schmidt number for self-mixing of turbulence	—	1	2
$\sigma_\epsilon$	turbulent Prandtl-Schmidt number for mixing of small-scale vorticity	—	1.3	2a
$\tau_\epsilon$	minimum of $\tau_{\text{free}}$ and $\tau_{\text{veg}}$	s		
$\tau_{\text{free}}$	dissipation time scale of free turbulence	s	equation (6)	
$\tau_{\text{veg}}$	dissipation time scale of eddies in between plants	s	equation (7)	
$L$	Size of eddies in between plants	m	equation (8)	
$C_{2\epsilon}$	scaling coefficient	—	1.96	2
$C_\mu$	scaling coefficient	—	0.09	2
$C_1$	scaling coefficient	—	0.8	2
$\epsilon_{s,x}, \epsilon_{s,y}, \epsilon_{s,z}$	eddy diffusivities in $x, y, z$ direction	$\text{m}^2 \text{s}^{-1}$	M	
$\epsilon_s$	sediment diffusion coefficient evaluated at the near bottom reference cell	$\text{m}^2 \text{s}^{-1}$	M	
$\tau$	bottom shear stress	$\text{N m}^{-2}$	M	
$C$	suspended sediment concentration	$\text{kg m}^{-3}$	M	
$C_a$	sediment reference concentration	$\text{kg m}^{-3}$	equation (9.3.4)	3



Table A2. (continued)

Symbol	Parameter	Unit	Value	Ref.
$c_{kmx}$	sediment reference concentration at the near bottom reference cell	$\text{kg m}^{-3}$	M	3
$w_s$	settling velocity of suspended sediment	$\text{m s}^{-1}$	$4.10^{-4}$	4
$E$	sediment erosion rate	$\text{kg m}^{-2} \text{s}^{-1}$	equation (12)	3
$D$	sediment deposition rate	$\text{kg m}^{-2} \text{s}^{-1}$	equation (12)	3
$\alpha_1$	correction factor	—	equation (12)	3
$\alpha_2$	correction factor for sediment concentration	—	equation (12)	3
$\Delta z$	difference in elevation between the center of the near bottom reference cell and the Van Rijn's reference height	m	equation (12)	3
$q_{s,x}$	suspended sediment transport flux in x-direction	$\text{kg m}^{-1} \text{s}^{-1}$	equation (13)	3
$q_{s,y}$	suspended sediment transport flux in y direction	$\text{kg m}^{-1} \text{s}^{-1}$	equation (13)	3
$q_x$	total transport in x-direction (including $q_{s,x}$ and bed load)	$\text{kg m}^{-1} \text{s}^{-1}$	equation (14)	3
$q_y$	total transport in y-direction (including $q_{s,y}$ and bed load)	$\text{kg m}^{-1} \text{s}^{-1}$	equation (14)	3
$\rho_s$	density	$\text{kg m}^{-3}$	equation (14)	3
$S$	the bed elevation changes includes erosion and deposition of sediment due to bed load and suspended load (source term Eq.14)	$\text{kg m}^{-2} \text{s}^{-1}$	equation (14)	4
$p_{\text{est}}$	stem density of initial established tussock	$\text{m}^{-2}$	$0.1^b$	5
$D$	Plant diffusion coefficient	$\text{m}^2 \text{y}^{-1}$	2	5
$r_1$	intrinsic growth rate of stem density	$\text{yr}^{-1}$	1	
$K_1$	maximum carry capacity of stem density	$\text{stems m}^{-2}$	800	1
$r_2$	intrinsic growth rate of stem height	$\text{m y}^{-1}$	2.5	6
$K_2$	maximum stem height	M	2.5	5
$h_{\text{est}}$	stem height of initial established tussock	M	$0.1^b$	5
$h_{\text{est}}$	stem height of initial established tussock	M	$0.1^b$	5
$h_b$	stem height; the stem height is included in F (Eq.1), it influences the sediment transport capacity by changing $u(z)$	M	M	
$PE_r$	plant mortality coefficient related to flow stress	$\text{m}^{-2} \text{s}^{-1}$	30	2
$\tau_{\text{cr},p}$	critical shear stress for plant mortality	$\text{N m}^{-2}$	0.26	7
$PE_H$	plant mortality coefficient related to flow stress	$\text{m}^{-3} \text{yr}^{-1}$	3000	2
$H$	Inundation height at high tide	M	M	
$H_{\text{cr},p}$	critical inundation height for plant mortality	M	1.8	5
$a$	scaling coefficient, scale to $\varphi(t_{\text{end}}) = \varphi_{\text{max}}$	—	equation (21)	
salt	salinity	ppt	35	5

<sup>a</sup>Description of parameter values of the model; Value = equation (x) means that this value is computed by a model equation; Value = M means that this value is computed by hydrodynamic model equations; References (Ref.) 1, Field assay Chongming Island in 2010; 2, Temmerman *et al.* [2007]; 3, van Rijn [1993]; 4, Lesser *et al.* [2004]; 5, Schwarz *et al.* [2011]; 6, Zhu *et al.* [2011]; 7, van Hulzen *et al.* [2007].

<sup>b</sup>Maximum value.

## Acknowledgments

This research was funded by the Sino-Dutch alliance PSA and by funds provided through the SKLEC 201001 project. We gratefully acknowledge the help of Cao Haobing, Chen Wangyi, Wang Ning, and Zhu Zhenchang at the State Key Laboratory for Estuarine and Coastal research in Shanghai. We greatly appreciate the comments of Bas van Maren and Bram van Prooijen at Deltares.

## References

- Allen, J. (2000), Morphodynamics of Holocene salt marshes: A review sketch from the Atlantic and Southern North Sea coasts of Europe, *Quat. Sci. Rev.*, 19(12), 1155–1231.
- Baptist, M. J. (2005), Modelling floodplain biogeomorphology, PhD thesis, TU Delft, Delft, The Netherlands.
- Baptist, M. J., V. Babovic, J. Rodriguez Uthurburu, M. Keijzer, R. E. Uittenbogaard, A. Mynett, and A. Verwey (2007), On inducing equations for vegetation resistance, *J. Hydraul. Res.*, 45(4), 435–450, doi:10.1080/00221686.2007.9521778.
- Bouma, T. J., L. A. van Duren, S. Temmerman, T. Claverie, A. Blanco-Garcia, T. Ysebaert, and P. M. J. Herman (2007), Spatial flow and sedimentation patterns within patches of epibenthic structures: Combining field, flume and modelling experiments, *Cont. Shelf Res.*, 27(8), 1020–1045, doi:10.1016/j.csr.2005.12.019.
- Bouma, T. J., M. Friedrichs, P. C. Klaassen, B. K. van Wesenbeeck, F. G. Brun, S. Temmerman, M. M. van Katwijk, G. Graf, and P. M. J. Herman (2009a), Effects of shoot stiffness, shoot size and current velocity on scouring sediment from around seedlings and propagules, *Mar. Ecol. Prog. Ser.*, 388, 293–297, doi:10.3354/meps08130.
- Bouma, T. J., M. Friedrichs, B. K. van Wesenbeeck, S. Temmerman, G. Graf, and P. M. J. Herman (2009b), Density-dependent linkage of scale-dependent feedbacks: A flume study on the intertidal macrophyte *Spartina anglica*, *Oikos*, 118(2), 260–268, doi:10.1111/j.1600-0706.2008.16892.x.
- Callaghan, D. P., T. J. Bouma, P. C. Klaassen, D. Van der Wal, M. J. F. Stive, and P. M. J. Herman (2010), Hydrodynamic forcing on salt-marsh development: Distinguishing the relative importance of waves and tidal flows, *Estuarine Coastal Shelf Sci.*, 89(1), 73–88, doi:10.1016/j.ecss.2010.05.013.
- D'Alpaos, A., S. Lanzoni, M. Marani, S. Fagherazzi, and A. Rinaldo (2005), Tidal network ontogeny: Channel initiation and early development, *J. Geophys. Res.*, 110, F02001, doi:10.1029/2004JF000182.
- D'Alpaos, A., S. Lanzoni, M. Marani, A. Bonorretto, G. Cecconi, and A. Rinaldo (2007), Spontaneous tidal network formation within a constructed salt marsh: Observations and morphodynamic modelling, *Geomorphology*, 91(3–4), 186–197, doi:10.1016/j.geomorph.2007.04.013.

- Defina, A., L. Carniello, S. Fagherazzi, and L. D'Alpaos (2007), Self-organization of shallow basins in tidal flats and salt marshes, *J. Geophys. Res.*, 112, F03001, doi:10.1029/2006JF000550.
- Dietrich, W. E., and J. T. Perron (2006), The search for a topographic signature of life, *Nature*, 439(7075), 411–418, doi:10.1038/nature04452.
- Fagherazzi, S., and T. Sun (2004), A stochastic model for the formation of channel networks in tidal marshes, *Geophys. Res. Lett.*, 31, L21503, doi:10.1029/2004GL020965.
- French, J. R., and D. Stoddart (1992), Hydrodynamics of salt marsh creek systems: Implications for marsh morphological development and material exchange, *Earth Surf. Processes Landforms*, 17(3), 235–252.
- Gabet, E. J. (1998), Lateral migration and bank erosion in a saltmarsh tidal channel in San Francisco Bay, California, *Estuaries*, 21(4), 745–753.
- Gao, J., F. Bai, Y. Yang, S. Gao, Z. Liu, and J. Li (2011), Influence of *Spartina* colonization on the supply and accumulation of organic carbon in tidal salt marshes of northern Jiangsu Province, China, *J. Coastal Res.*, 28(2), 486–498, doi:10.2112/JCOASTRES-D-11-00062.1.
- Gran, K., and C. Paola (2001), Riparian vegetation controls on braided stream dynamics, *Water Resour. Res.*, 37(12), 3275–3283.
- Hickin, E. J. (1984), Vegetation and river channel dynamics, *Can. Geogr.*, 28(2), 111–126.
- Hood, W. G. (2006), A conceptual model of depositional, rather than erosional, tidal channel development in the rapidly prograding Skagit River Delta (Washington, USA), *Earth Surf. Processes Landforms*, 31(14), 1824–1838, doi:10.1002/esp.1381.
- Jones, C., J. H. Lawton, and M. Shachak (1994), Organisms as ecosystem engineers, *Oikos*, 69, 373–386.
- Kirwan, M. L., and A. B. Murray (2007), A coupled geomorphic and ecological model of tidal marsh evolution, *Proc. Natl. Acad. Sci. U. S. A.*, 104(15), 6118–6122, doi:10.1073/pnas.0700958104.
- Leonard, L. A., and A. L. Croft (2006), The effect of standing biomass on flow velocity and turbulence in *Spartina alterniflora* canopies, *Estuarine Coastal Shelf Sci.*, 69(3), 325–336, doi:10.1016/j.ecss.2006.05.004.
- Lesser, G. R., J. A. Roelvink, J. Van Kester, and G. S. Stelling (2004), Development and validation of a three-dimensional morphological model, *Coastal Eng.*, 51(8), 883–915, doi:10.1016/j.coastaleng.2004.07.014.
- López, F., and M. García (1998), Open-channel flow through simulated vegetation: Suspended sediment transport modeling, *Water Resour. Res.*, 34(9), 2341–2352.
- Marani, M., S. Lanzoni, D. Zandolin, G. Seminara, and A. Rinaldo (2002), Tidal meanders, *Water Resour. Res.*, 38(11), 1225, doi:10.1029/2001WR000404.
- Marciano, R., Z. B. Wang, A. Hibma, H. J. de Vriend, and A. Defina (2005), Modeling of channel patterns in short tidal basins, *J. Geophys. Res.*, 110, F01001, doi:10.1029/2003JF000092.
- Mudd, S., A. D'Alpaos, and J. Morris (2010), How does vegetation affect sedimentation on tidal marshes? Investigating particle capture and hydrodynamic controls on biologically mediated sedimentation, *J. Geophys. Res.*, 115, F03029, doi:10.1029/2009JF001566.
- Nepf, H. M. (1999), Drag, turbulence, and diffusion in flow through emergent vegetation, *Water Resour. Res.*, 35(2), 479–489.
- Nepf, H. M. (2012), Hydrodynamics of vegetated channels, *J. Hydraul. Res.*, 50(3), 262–279, doi:10.1080/00221686.2012.696559.
- Perillo, G. M. E., E. Wolanski, and D. R. Cahoon (2009), *Coastal wetlands: An Integrated Ecosystem Approach*, Elsevier Science, Amsterdam.
- Pestrong, R. (1965), The development of drainage patterns on tidal marshes, *Stanford Univ. Publ.*, 10(2), 1–87.
- Pestrong, R. (1972), Tidal-flat sedimentation at cooley landing, Southwest San Francisco bay, *Sediment. Geol.*, 8(4), 251–288.
- Prosser, I. P., and C. J. Slade (1994), Gully formation and the role of valley-floor vegetation, southeastern Australia, *Geology*, 22(12), 1127–1130.
- Redfield, A. (1965), Ontogeny of a salt marsh estuary, *Science*, 147(3653), 50–55.
- Rietkerk, M., M. C. Boerlijst, F. van Langevelde, R. HilleRisLambers, J. van de Koppel, L. Kumar, H. H. Prins, and A. M. de Roos (2002), Self-organization of vegetation in arid ecosystems, *Am. Nat.*, 160(4), 524–530, doi:10.1086/342078.
- Rinaldo, A., I. Rodriguez-Iturbe, and R. Rigon (1998), Channel networks, *Annu. Rev. Earth Planet. Sci.*, 26(1), 289–327.
- Rodgers, J. L., and W. A. Nicewander (1988), Thirteen ways to look at the correlation coefficient, *Am. Stat.*, 42(1), 59–66.
- Roelvink, J. A., and G. van Banning (1995), Design and development of DELFT3D and application to coastal morphodynamics, *Oceanogr. Lit. Rev.*, 42(11), 451–456.
- Schwarz, C., T. Ysebaert, Z. Zhu, L. Zhang, T. J. Bouma, and P. M. J. Herman (2011), Abiotic factors governing the establishment and expansion of two salt marsh plants in the Yangtze estuary, China, *Wetlands*, 31(6), 1011–1021, doi:10.1007/s13157-011-0212-5.
- Steel, T., and K. Pye (1997), The development of salt marsh tidal creek networks: Evidence from the UK, paper presented at Proceedings of the Canadian Coastal Conference.
- Steers, J. A. (1960), in *Physiography and Evolution of Scott Head Island*, edited by J. A. Steers, pp. 12–66, W. Heffer, Cambridge.
- Stefanon, L., L. Carniello, A. D'Alpaos, and S. Lanzoni (2010), Experimental analysis of tidal network growth and development, *Cont. Shelf Res.*, 30(8), 950–962, doi:10.1016/j.csr.2009.08.018.
- Tal, M., and C. Paola (2007), Dynamic single-thread channels maintained by the interaction of flow and vegetation, *Geology*, 35(4), 347–350, doi:10.1130/G23260A.1.
- Temmerman, S., T. J. Bouma, G. Govers, Z. B. Wang, M. B. De Vries, and P. M. J. Herman (2005), Impact of vegetation on flow routing and sedimentation patterns: Three-dimensional modeling for a tidal marsh, *J. Geophys. Res.*, 110, F04019, doi:10.1029/2005JF000301.
- Temmerman, S., T. J. Bouma, J. Van de Koppel, D. D. Van der Wal, M. B. De Vries, and P. M. J. Herman (2007), Vegetation causes channel erosion in a tidal landscape, *Geology*, 35(7), 631–634, doi:10.1130/g23502a.1.
- Uittenbogaard, R. E. (2003), Modelling turbulence in vegetated aquatic flows, paper presented at International workshop on RIParian FORest vegetated channels: hydraulic, morphological and ecological aspects, Trento, Italy.
- van de Koppel, J., D. van der Wal, J. P. Bakker, and P. M. J. Herman (2005), Self-organization and vegetation collapse in salt marsh ecosystems, *Am. Nat.*, 165(1), E1–E12, doi:10.1086/426602.
- van der Wal, D., and P. M. J. Herman (2012), Ecosystem engineering effects of *Aster tripolium* and *Salicornia procumbens* salt marsh on macrofaunal community structure, *Estuaries Coasts*, 35, 714–726, doi:10.1007/s12237-011-9465-8.
- van der Wal, D., A. Wielemaker-Van den Dool, and P. M. J. Herman (2008), Spatial patterns, rates and mechanisms of saltmarsh cycles (Westerschelde, The Netherlands), *Estuarine Coastal Shelf Sci.*, 76(2), 357–368, doi:10.1016/j.ecss.2007.07.017.
- van Hulzen, J., J. Van Soelen, and T. Bouma (2007), Morphological variation and habitat modification are strongly correlated for the autogenic ecosystem engineer *Spartina anglica* (common cordgrass), *Estuaries Coasts*, 30(1), 3–11, doi:10.1007/BF02782962.
- van Ledden, M., W. G. M. van Kesteren, and J. C. Winterwerp (2004), A conceptual framework for the erosion behaviour of sand-mud mixtures, *Cont. Shelf Res.*, 24(1), 1–11, doi:10.1016/j.csr.2003.09.002.
- van Maanen, B., G. Coco, and K. R. Bryan (2013), Modelling the effects of tidal range and initial bathymetry on the morphological evolution of tidal embayments, *Geomorphology*, 191, 23–34, doi:10.1016/j.geomorph.2013.02.023.
- van Rijn, L. C. (1993), *Principles of Sediment Transport in Rivers, Estuaries and Coastal Seas*, Aqua publications Amsterdam, Amsterdam.
- van Wesenbeeck, B. K., J. van de Koppel, P. M. J. Herman, M. D. Bertness, D. van der Wal, J. P. Bakker, and T. J. Bouma (2008), Potential for sudden shifts in transient systems: Distinguishing between local and landscape-scale processes, *Ecosystems*, 11(7), 1133–1141, doi:10.1007/s10021-008-9184-6.

- Vandenbruwaene, W., S. Temmerman, T. J. Bouma, P. C. Klaassen, M. B. De Vries, D. P. Callaghan, P. Van Steeg, F. Dekker, L. A. Van Duren, and E. Martini (2011), Flow interaction with dynamic vegetation patches: Implications for biogeomorphic evolution of a tidal landscape, *J. Geophys. Res.*, *116*, F01008, doi:10.1029/2010JF001788.
- Vandenbruwaene, W., T. J. Bouma, P. Meire, and S. Temmerman (2012), Bio-geomorphic effects on tidal channel evolution: Impact of vegetation establishment and tidal prism change, *Earth Surf. Processes Landforms*, *38*(2), 122–132, doi:10.1002/esp.3265.
- Vlaswinkel, B. M., and A. Cantelli (2011), Geometric characteristics and evolution of a tidal channel network in experimental setting, *Earth Surf. Processes Landforms*, *36*(6), 739–752, doi:10.1002/esp.2099.
- Wang, Z. B., T. Louters, and H. J. De Vriend (1995), Morphodynamic modelling for a tidal inlet in the Wadden Sea, *Mar. Geol.*, *126*(1), 289–300.
- Xu, G., and R. Zhuo (1985), Preliminary studies of introduced *Spartina alterniflora* Loisel in China (I), *J. Nanjing Univ. (Res. Adv. Spartina: Achiev. of Past 22 Years)*, *1*, 212–225.
- Yang, S. L., J. D. Milliman, P. Li, and K. Xu (2011), 50,000 dams later: Erosion of the Yangtze River and its delta, *Global Planet. Change*, *75*(1), 14–20, doi:10.1016/j.gloplacha.2010.09.006.
- Ye, Q. (2012), An approach towards generic coastal geomorphological modelling with applications, PhD thesis, TU Delft, Delft, The Netherlands.
- Zhu, Z., L. Zhang, N. Wang, C. Schwarz, and T. Ysebaert (2011), Interactions between the range expansion of saltmarsh vegetation and hydrodynamic regimes in the Yangtze estuary, China, *Estuarine Coastal Shelf Sci.*, *96*(1), 273–279, doi:10.1016/j.ecss.2011.11.027.